



HAL
open science

**Inelastic neutron scattering study of the lattice
dynamics of the homologous compounds
(PbSe)₅(Bi₂Se₃)_{3m} (m = 1, 2 and 3)**

Selma Sassi, Christophe Candolfi, Anne Dauscher, Bertrand Lenoir, Michael
Marek Koza

► **To cite this version:**

Selma Sassi, Christophe Candolfi, Anne Dauscher, Bertrand Lenoir, Michael Marek Koza. Inelastic neutron scattering study of the lattice dynamics of the homologous compounds (PbSe)₅(Bi₂Se₃)_{3m} (m = 1, 2 and 3). *Physical Chemistry Chemical Physics*, 2018, 20 (21), pp.14597-14607. 10.1039/c8cp01277f. hal-02391383

HAL Id: hal-02391383

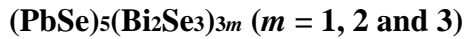
<https://hal.science/hal-02391383>

Submitted on 24 Mar 2020

HAL is a multi-disciplinary open access archive for the deposit and dissemination of scientific research documents, whether they are published or not. The documents may come from teaching and research institutions in France or abroad, or from public or private research centers.

L'archive ouverte pluridisciplinaire **HAL**, est destinée au dépôt et à la diffusion de documents scientifiques de niveau recherche, publiés ou non, émanant des établissements d'enseignement et de recherche français ou étrangers, des laboratoires publics ou privés.

Inelastic neutron scattering study of the lattice dynamics of the homologous compounds



Selma Sassi¹, Christophe Candolfi^{1,*}, Anne Dauscher¹, Bertrand Lenoir¹, Michael Marek

Koza²

¹Institut Jean Lamour, UMR 7198 CNRS – Université de Lorraine, 2 allée André Guinier-Campus ARTEM, BP 50840, 54011 Nancy Cedex, France

²Institut Laue Langevin, 6 rue Jules Horowitz, B.P. 156, 38042 Grenoble, Cedex 9, France

*Contact author: christophe.candolfi@univ-lorraine.fr

Abstract

We report on the inelastic response of the homologous compounds $(\text{PbSe})_5(\text{Bi}_2\text{Se}_3)_{3m}$ for $m = 1, 2$ and 3 followed in a broad temperature range (50 – 500 K) using high-resolution powder inelastic neutron scattering experiments. These results are complemented by low-temperature measurements of the specific heat (2 – 300 K). The evolution of the anisotropic crystal structure of these compounds with varying m , built from alternate Pb-Se and m Bi-Se layers, only weakly influences the generalized phonon density of states. In all the three compounds, intense inelastic signals, likely mainly associated with the dynamics of the Pb atoms, are observed in the 4.5 – 6 meV low-energy range. The response of these low-energy modes to temperature variations indicates a conventional quasi-harmonic behavior over the whole temperature range investigated. The modes located above 8 meV show a minor temperature effect regardless of the value of m . The low-energy excess of vibrational modes manifests itself in the low-

temperature specific heat as a pronounced peak in the $C_p(T)/T^3$ data near 10 K. The lack of significant anharmonicity beyond that associated with the thermal expansion of the lattice suggests that the inherent disorder in the monoclinic unit cell and scattering at interlayer interfaces are the most important ingredients that limit the heat transport in this series of compounds.

I. Introduction

Homologous compounds are interesting families of materials, the crystal structure of which can be rationalized by the presence of one or several types of building blocks of various dimensions.¹⁻³ The number of each of these structural units is described by integer or half-integer numbers in their chemical formula. Foreign elements can be often inserted in empty voids or intercalated between layers and can act as dopants or help to stabilize the crystal structure.¹⁻³ Most of these materials crystallize with a low-symmetry structure that gives rise to anisotropic transport properties. The inherent disorder present in their unit cell makes these compounds an interesting area of research for designing materials with low lattice thermal conductivity, κ_L , for thermoelectric applications or for searching for novel compounds with topologically non-trivial electronic band structure.⁴⁻¹³

Both topological surface states and interesting thermoelectric properties were indeed evidenced in the series of homologous compounds $(\text{PbSe})_5(\text{Bi}_2\text{Se}_3)_{3m}$ ($1 \leq m \leq 4$) for $m = 2$ and $m = 1, 2$ and 3 , respectively.⁶⁻¹⁶ This series is built from an ordinary insulator (PbSe) and a topological insulator (Bi_2Se_3), both of which are well-known narrow-band-gap semiconductors with good thermoelectric performances.^{17,18} The crystal structure of these homologous compounds is formed by alternating Pb-Se and m Bi-Se layers stacked along the a axis of the monoclinic unit cell described in the space groups $P2_1/m$ ($m = 1$ and 3), $C2/m$ ($m = 2$) or $P2/m$

($m = 4$) (Figure 1).^{8,9,14-16} In all compounds, Pb atoms are surrounded by Se atoms which form complex distorted polyhedra while Bi atoms are located at the centre of distorted Se octahedra (Figure 1). These compounds exhibit semiconducting-like ($m = 1$) or metallic-like ($m = 2, 3$ and 4) electrical properties with optical band gaps varying between 0.35 and 0.40 eV.^{8,9,14-16} As expected from their complex crystal structure, these compounds possess a low ability to transport heat with lattice thermal conductivity values as low as 0.3 W m⁻¹ K⁻¹ at 723 K.^{6,8,14-16} In addition to these extremely low values, another ingredient making this series worthy of further investigations is the unusual dependence of κ_L on the structural complexity of the unit cell controlled by the integer m . Synonymous with increasing the structural complexity, increasing m does not lead to a decrease in κ_L but to the opposite trend.⁸ The presence of numerous defects and stacking faults in their microstructure, the active lone pair electrons of the Pb and Bi atoms responsible for distortions in their local chemical environments and the number of interfaces between both types of layers are all important traits that may contribute to lower κ_L and explain its unusual variation with m . Another degree of complexity is added by the large anisotropic thermal vibrations of the Pb atoms evidenced by single-crystal X-ray diffraction which are expected to give rise to low-lying optical modes.^{8,19} These modes might behave anharmonically upon temperature variations and thus, enhance the occurrence of three-phonon Umklapp processes, thereby significantly reducing the lifetime of acoustic phonons as demonstrated in several materials with complex crystal structures.²⁰⁻²⁴

Here, we probe this last possibility by investigating in detail the lattice dynamics of the stable $m = 1, 2$ and 3 members of this series through a combination of time-of-flight powder inelastic neutron scattering (INS) measurements of the generalized vibrational density of states (GVDOS) between 50 and 500 K and low-temperature specific heat measurements (2 – 300 K). Our results show that the overall features of the GVDOS are only weakly affected upon increasing m . The inelastic response is dominated at low energies by vibrational modes centred

near 4.8 meV likely associated with the thermal motion of the Pb atoms. For all compounds, the temperature response of the GVDOS is indicative of a quasi-harmonic behaviour with no evident signs of anharmonicity beyond that related to thermal expansion. This absence indicates that the anharmonicity is not sufficient to solely account for the observed very low, glass-like lattice thermal conductivity and suggests that static effects related to disorder and lattice mismatch between both types of layers play a prominent role in determining the thermal transport and its unusual evolution with m .

II. Experimental section

A. Sample preparation and characterization

Polycrystalline $(\text{PbSe})_5(\text{Bi}_2\text{Se}_3)_{3m}$ samples with $m = 1, 2$ and 3 were prepared by a two-step synthetic approach according to the pseudo-binary $\text{PbSe} - \text{Bi}_2\text{Se}_3$ phase diagram.^{6-8,14-16} First, the binaries PbSe and Bi_2Se_3 were synthesized by direct reaction of the elements sealed in evacuated quartz tubes. The tubes were placed in a rocking furnace, heated at 1393 K, dwelt at this temperature for 12 h before being cooled to room temperature over 2 h. In a second step, the two ingots were hand-ground into fine powders (particle size $< 100 \mu\text{m}$), weighted in stoichiometric quantities and pelletized. The pellets were sealed in evacuated quartz ampules and annealed at 873 K for 10 days to obtain the $m = 1, 2$ and 3 compounds.

The crystal structure was verified by powder X-ray diffraction (PXRD) at 300 K (Cu $K\alpha_1$ radiation, $\lambda = 1.54056 \text{ \AA}$) using a Bruker D8 Advance diffractometer. In agreement with prior studies,⁶⁻⁸ no obvious impurities could be detected to within the detection limits of PXRD. Note that prior X-ray analyses on single crystals have suggested that deviations from ideality in these systems may be present.⁸ In particular, a mixed occupancy of Pb and Bi on some of the Pb sites

is very likely giving rise to an enhanced disorder in the unit cell. This inherent characteristic of these compounds does not change our interpretation of the INS data and main conclusions presented below. Hereafter, we will consider nevertheless a structural model where the Pb and Bi atoms occupy distinct layers as commonly used in the literature.⁶⁻¹⁶

B. Inelastic neutron scattering experiments

INS experiments were performed at the thermal neutron and cold neutron time-of-flight spectrometers IN4 and IN6, respectively, located at the Institut Laue Langevin (Grenoble, France). The inelastic response was recorded on IN6@ILL in the time-focusing mode with the best energy resolution set to 7.5 meV at the anti-Stokes line. IN4@ILL spectrometer was used to extend the energy-momentum phase-space covered by IN6 and to monitor the inelastic response of the samples at the Stokes line down to 50 K. All measurements were carried out in cryostats in helium atmosphere of about 10 mbar. Incident neutron wavelengths of 4.14 and 2.20 Å were used on IN6 and IN4, respectively.

The powdered samples, of about 15g each, were placed in a niobium cylinder can. The measurements were conducted at $T \approx 100, 300$ and 500 K on IN6 and at various temperatures between 50 and 300 K on IN4. Standard procedures for data correction and conversion were considered.²⁵ More specifically, the data were corrected for empty sample holder scattering, for absorption, for frame overlap and self-attenuation and for different detector efficiencies of the multidetector banks. Because of the difference in scattering powers between the Pb/Bi and Se atoms (0.0536, 0.0438 and 0.105 barns/amu for Pb, Bi and Se, respectively),²⁶ the present INS measurements are more sensitive to the Se atoms.

The dynamic structure factors $S(Q, \omega, T)$ were calculated as an average signal over the scattering angle and have been corrected for the Bose-Einstein thermal occupation number in

order to highlight the effect of the Debye-Waller factors on the dynamic response functions. The Q -averaged generalized vibrational density of states $G(\omega)$ was derived within the incoherent approximation formalism.²⁷⁻³⁰ Attempts at applying a self-consistent multiphonon correction using the MuPhoCor software were performed by approximating the masses and cross sections of the sample constituents by values averaged over the properties of the compounds. Because this approach is in principle strictly applicable for monoatomic systems, this procedure did not yield well-converged corrections. However, since the contribution of the n th phonon term ($n = 1, 2, 3, \dots$) to the inelastic signal is proportional to $(Q^2/m)^2$, with m the mass of the scatterers, the multiphonon terms are expected to be very weak in the case of heavy-mass compounds. For these reasons, all the spectra presented hereafter have not been corrected for multiphonon contributions. All the spectra have been normalized so that the integral of $G(\omega)$ corresponds to 75, 120 and 165 phonon modes for the $m = 1, 2$ and 3 compound, respectively. The peak positions of the modes observed in $G(\omega)$ were approximated by Gaussian least-squares fits. For the IN4 data, only fits to the Stokes line were considered due to the lack of resolution at the anti-Stokes line. For the IN6 data, only the anti-Stokes line was analysed due to the limited energy range accessible by this spectrometer at the Stokes line.

C. Specific heat measurements

The specific heat C_p was measured between 2 and 300 K with a physical property measurement system (PPMS, Quantum Design) using a conventional relaxation method. Small polycrystalline bulk pieces of the $m = 1, 2$ and 3 compounds of approximately 20 mg were glued with a tiny amount of Apiezon N grease to ensure a good thermal coupling between the sample and the specific heat puck.

III. Results and discussion

A. Generalized density of states at 300 K

The dynamic structure factor $S(Q, \omega)$ measured at IN6@ILL is shown in Figure 2. A number of excitations are clearly visible as strong intensity regions. The rising intensity with increasing Q is characteristic of the phonon form factor weighted by the coherent scattering power of the sample constituents. Upon averaging, this coherent phonon response scales approximately as Q^2 . At low energies, dispersions of acoustic modes, marked by horizontal white arrows in Figure 2, emanate from intense Bragg peaks located at the elastic line at zero energy transfer. The $S(Q, \omega)$ maps are similar for all the three compounds with three main regions of intensity visible near 5, 10 and 15 meV.

A comparison of the generalized density of states $G(\omega)$ of the three compounds derived from the aforementioned $S(Q, \omega)$ maps is shown in Figure 3a. All the spectra exhibit prominent common features indicating that the number of Bi-Se layers only influences the details of the lattice dynamics in this series of compounds. The low-energy part of the spectra below 10 meV is dominated by a pronounced peak centred at around 5 meV followed by an intensity trough at 7 meV. Above this energy, the inelastic signal is dominated by several maxima that extend between 7 meV and 12 meV. A third broad block composed of several maxima and shoulders is observed up to the energy cut-off of around 20 meV. The influence of the m BiSe layers becomes obvious in the relative intensities of the maxima in this spectral fine structure. Thereby, they are better defined and distinguished with higher m . For instance, we note the split of the spectral density between 7 and 12 meV, which appears to be smeared out in the $m = 1$ compound, into two peaks centred around 8 and 11 meV for the $m = 3$ structure. At the highest energies, that is, above 15 meV, the intensity maximum of this block tends to shift towards

higher energies with increasing m . Another important difference between the three spectra is tied to the shoulder near 6 meV which is better resolved in the $m = 3$ compound while only a broad peak at 5 meV is visible for $m = 1$ and 2.

A precise assignment of these peaks to modes dominated by the motion of Pb, Bi or Se atoms is not straightforward in the absence of lattice dynamics calculations. However, as observed in numerous families of cage-like compounds,³¹⁻³⁷ the thermal motion of the atoms that exhibit the highest anisotropic thermal displacement parameters (ADP) gives rise to features that dominate the low-energy inelastic response. Thus, it seems reasonable to posit a similar mode assignment in the present case. Single-crystal X-ray diffraction data collected at 300 K on the three compounds have indicated that the Pb atoms exhibit the highest ADP values followed by the Bi atoms and eventually, the Se atoms.⁸ Of note, some of the Bi atoms feature nearly equivalent, although slightly lower, ADP values to those of the Pb atoms.⁸ In this context, the low-energy peak at around 5 meV is probably mainly dominated by the contribution of the Pb atoms with some admixture of Bi-weighted contributions. Further following this line, the two blocks of peaks at higher energies would be then mainly dominated by the contributions of Bi and Se atoms. Because of the mass contrast between Bi and Se atoms, the latter are expected to show the highest vibration frequencies giving rise to Se-weighted modes dominating the high energy part of the spectra.

The link between the low-energy peak and Pb-weighted modes is further supported by the equivalent thermal displacement parameters U_{eq} determined by single-crystal X-ray diffraction (see Table 1).⁸ Assuming that the thermal motion of the Pb atoms in their respective polyhedron can be described by a harmonic oscillator model corresponding to an Einstein mode, an estimate of the vibrational frequency ν can be inferred at 300 K using the high-temperature limit of the temperature dependence of U_{eq} given by the relation $U_{eq} = k_B T / [m(2\pi\nu)^2]$, where k_B is the Boltzmann constant and m is the mass of Pb.³⁸ From the values of ν , characteristic Einstein

temperatures $\theta_E = hv/k_B$ (h is the Planck constant) ranging between 48 and 57 K are obtained for the $m = 1$ compound. The lower and upper limits of this range are associated with the Pb5 and Pb1 atoms, respectively. The θ_E derived for the $m = 2$ and 3 compounds fall within a similar range with the lowest θ_E value decreasing from 48 to 44 K on going from $m = 1$ to $m = 3$ while, meanwhile, the highest limit increases up to 60 K. These Einstein temperatures correspond to characteristic energies ranging between 3.8 and 5.1 meV that agree very well with the low-energy maxima observed in $G(\omega)$ (see Figure 3a).

The close agreement between this simple model and the low-energy features observed in the phonon spectra can be better appreciated in the corresponding Debye plot $G(\omega)/\omega^2$ versus $\hbar\omega$, shown in Figure 3b. These data evidence that the low-energy peak is in fact composed of a first shoulder at 3.7 meV followed by another peak at 4.8 meV for all compounds. While these two characteristic energies are in agreement with the aforementioned Einstein temperatures derived for the Pb atoms, it cannot be strictly excluded, however, that the lowest peak observed near 3.7 meV is related to zone-boundary modes with low group velocity values.

In order to further shed light on the influence of the number of Bi-Se layers m on the lattice dynamics, Figure 4 shows the Debye plot of the difference signal $\Delta G(\omega, 300K) = G_{m=3}(\omega, 300K) - G_{m=1}(\omega, 300K)$ obtained after normalizing the spectra of the $m = 1$ and $m = 3$ compounds to the signal from acoustic phonons, that is, below 4 meV. This difference spectrum indicates a higher spectral density at 4.8 and 6 meV indicating that the two additional Bi-Se layers also contribute to the inelastic response of the low-energy localized modes. Indeed, within an Einstein scenario, the highest U_{eq} values of the Bi atoms would correspond to characteristic energies increasing from 5.2 meV in the $m = 1$ compound up to 6.9 meV in the $m = 3$ compound. The development of the shoulder at 6 meV upon increasing m may thus reflect a more pronounced contribution of the Bi-Se layers to the inelastic signal around this energy.

B. Temperature dependence of the generalized density of states

Figure 5 presents the dynamic structure factor $S(Q, \omega)$ of the $m = 1$ and 3 compounds, recorded at 100 and 300 K at IN4@ILL. The strong increase in the inelastic intensity at 300 K is a direct consequence of the Bose thermal occupation number. Van Hove singularities observed in $G(\omega)$ inferred from the IN6 data at 300 K are indicated by horizontal white arrows while acoustic phonons emanating from strong Bragg peaks are indicated by vertical arrows. At 300 K, the signals of both compounds features intensity maxima located in distinct regions of the $S(Q, \omega)$ maps and are consistent with those recorded on the IN6 spectrometer. No significant variations in intensity between the maps of the $m = 1$ and 3 compounds are evidenced. Upon cooling, the characteristic energies of the regions of high intensity do not experience a significant shift. In particular, the lack of strong temperature dependence of the lowest-energy spot suggests the absence of significant anharmonicity in both compounds.

This last statement is further corroborated by the temperature responses of $G(\omega)$ for the three compounds (Figure 6). The panels show a direct comparison of the IN4 and IN6 data in the full energy range taken at the Stokes and anti-Stokes line, respectively, with the corresponding Debye plots restricted to the low-energy region presented in Figure 7. While both data sets are consistent with each other, some subtle differences in $G(\omega)$ are present due to differences in phase-space coverage and resolution of the two spectrometers. The main temperature effect observed is a shift of the entire spectra towards lower energies upon heating. This shift is characteristic of the thermal expansion of the unit cell indicative of anharmonic behaviour usually referred to as quasi-harmonic. The observed decrease in the intensity of the inelastic signal upon heating is a direct consequence of the concomitant increase in the Debye-Waller factors. The effect of temperature on the low-energy peak at 4.8 meV is nearly similar in all the three compounds (see Figure 7) with no evident change in the temperature range

covered. The data below 2 meV have been discarded due to the strong increase in the measured intensity that originates from the elastic contribution of the Bragg peaks which is of increasing importance as the inelastic signal is reduced upon cooling.

To further quantify the energy shift of the low-energy peaks as a function of the temperature, the $G(\omega)/\omega^2$ data have been modelled by a function with up to two Gaussians and a background term following the relation $G(\omega)/\omega^2 = a + be^{-cE} + \sum_{i=1}^2 A_i \exp\left(-\frac{(E-E_i)^2}{2\sigma_i^2}\right)$ where the coefficients a , b and c are fitting parameters to describe the background and A_i , E_i and σ_i are the amplitude, the characteristic energy and the standard deviation of the Gaussians, respectively. For the IN6 data, a flat background term was used so that b was set to zero in the whole temperature range. For the IN4 data, the first exponential term was used to approximate the Bragg peaks contribution and the parameters a , b and c were fitted with one Gaussian function to describe the low-energy peak.

The temperature dependence of the characteristic energy of the main low-energy peak at 4.8 meV is shown in Figure 8. For all compounds, this peak experiences a slight decrease in its characteristic energy upon heating consistent with a conventional quasi-harmonic behaviour. This conventional temperature dependence contrasts with those observed in tetrahedrites $\text{Cu}_{12}\text{Sb}_4\text{S}_{13}$, pyrochlores $\text{A}_2\text{Os}_2\text{O}_6$ ($A = \text{K}, \text{Rb}, \text{Cs}$) or in the Einstein solids $\text{MV}_2\text{Al}_{20}$ ($M = \text{Sc}, \text{Al}, \text{Ga}$) where the low-energy excess of vibrational modes significantly shifts towards higher energies upon heating, indicative of a high degree of anharmonicity induced by flat bottom or double-well potentials.³⁹⁻⁴⁵ The lack of such anharmonicity in the present series of compounds further suggests the absence of anharmonic terms in the potential felt by the Pb atoms beyond the conventional cubic term characteristic of the thermal expansion of the lattice.

C. Specific heat

The low-energy features of the GVDOS spectra related to optical phonons or zone-boundary excitations leave signatures in momentum and energy-averaged responses such as thermal displacement parameters or specific heat. In the latter thermodynamic property, the departure of the GVDOS from a ω^2 dependence at low energies leads to an excess specific heat that exceeds the Debye contribution at low temperatures when the specific heat $C_p(T)$ data are plotted as C_p/T^3 versus T . As shown in Figure 9, pronounced maxima centered at 10 K are conclusively observed in all the three compounds. In cage-like materials such as clathrates, the weakly-bonded guest atoms give rise to partial phonon density of states concentrated in a narrow energy window at low energies. In such a case, a one-to-one correspondence is obtained between the low-energy peaks in the phonon spectra and the characteristic Einstein temperatures inferred from the temperature dependence of U_{eq} .⁴⁶⁻⁵³ When such a correspondence holds, the excess specific heat can be then adequately modelled by a linear combination of Debye and Einstein terms.⁴⁶⁻⁵³ Here, we tried to model similarly the specific heat data of the present series of compounds by considering the following relation

$$C_p(T) \approx C_v(T) = C_D(T) + C_{E1}(T) + C_{E2}(T) \quad (1)$$

where $C_D(T)$ and $C_{Ei}(T)$ are the lattice specific heat within the Debye approximation and the Einstein contribution of the localized oscillators i , respectively, given by

$$C_D(T) = 9N_D R \left(\frac{T}{\theta_D}\right)^3 \int_0^{\theta_D/T} \frac{x^4 e^x}{(e^x - 1)^2} dx \quad (2)$$

$$C_{Ei}(T) = p_i N_{Ei} R \left(\frac{\theta_{Ei}}{T} \right)^2 \frac{e^{\theta_{Ei}/T}}{(e^{\theta_{Ei}/T} - 1)^2} \quad (3)$$

In these two expressions, R is the gas constant, N_D is the number of Debye oscillators per formula unit, p_i and N_{Ei} are the spectral weight and the number of the Einstein oscillators i and θ_D is the Debye temperature. The fitting parameters obtained for various models are given in Table 2. For the $m = 1$ and 2 compounds, models with one or two Einstein temperatures were considered with the spectral weights either allowed to vary or set to $p_1 N_{E1} = 3$ and $p_2 N_{E2} = 2$ to reflect the anisotropic, mainly one-dimensional ADP values of the Pb atoms. As shown in Figure 9, these simple models describe well the low-temperature data up to around 20 K. In particular, the results evidence that one Einstein temperature is sufficient to describe the temperature dependence of the specific heat when the spectral weight is allowed to vary. On going from $m = 1$ to $m = 2$, $p_1 N_{E1}$ increases from ≈ 3.6 to ≈ 6 . This variation is further observed in the $m = 3$ compound for which, the spectral weight increases to $p_1 N_{E1} \approx 8$. The observed trend in the spectral weight with increasing m might reflect the less anisotropic, more three-dimensional thermal motions of the Pb atoms in the $m = 3$ compound compared to $m = 1$ as indicated by single-crystal X-ray diffraction data. Alternatively, this increase may also be a consequence of the more pronounced contribution of the Bi atoms in this energy region due to the additional Bi-Se layers. As observed in the two other members of this series, a second Einstein temperature does not significantly improve the quality of the fit. At higher temperatures, however, none of the models capture entirely the temperature dependence of the specific heat. While the fit is reasonable in the $m = 1$ compound, its quality worsens with increasing m . This shortcoming reflects the inadequacy of a single Debye temperature to describe adequately the contributions at higher temperatures of the large number of optic modes that originate from the large number of atoms in the unit cell. Regardless of the model considered, the best fit values for the Einstein temperatures are consistent with both the

aforementioned analysis of the INS data and the U_{eq} values for which characteristic Einstein temperatures ranging between 44 and 60 K have been derived. This good agreement confirms the presence of low-energy, Einstein-like modes associated with the Pb atoms and further indicates that the partial vibrational density of states of Pb and possibly Bi are localized within a narrow energy band at low energies.

IV. Summary and conclusion

The lattice dynamics of the homologous series of compounds $(\text{PbSe})_5(\text{Bi}_2\text{Se}_3)_{3m}$ ($m = 1, 2$ and 3) has been explored in detail by temperature-dependent inelastic neutron scattering and specific heat measurements. The overall inelastic response exhibits pronounced features independent of the value of m , dominated by a broad low-energy peak around 4.8 meV that is likely at the origin of the large thermal displacements of the Pb atoms about their equilibrium positions. This low-energy structure manifests itself in the specific heat giving rise to an excess contribution at low temperatures fairly well described by a simple model combining Debye and Einstein-like terms. The temperature response of the inelastic signal, followed from 50 up to 500 K, reveals a slight decrease in the characteristic energy of this low-energy excess indicative of a conventional quasi-harmonic behavior that suggests the absence of strong anharmonicity beyond that tied to the thermal expansion of the lattice. This absence further corroborates the assumption that the interfaces between the Pb-Se and Bi-Se layers play a key role in phonon scattering in this series of layered compounds.

Conflicts of interest

There are no conflicts of interest to declare.

Acknowledgements

The authors acknowledge the ILL College 7 for the support of this work and the grant of accessing the instruments of the European neutron source facilities at the Institut Laue Langevin in Grenoble (France).

References

- 1 G. Tan, L.-D. Zhao and M. G. Kanatzidis, *Chem. Rev.*, 2016, **116**, 12123–12149.
- 2 A. Mroczek and M. G. Kanatzidis, *Acc. Chem. Res.*, 2003, **36**, 111–119.
- 3 M. G. Kanatzidis, *Acc. Chem. Res.*, 2005, **38**, 359–368.
- 4 A. Olvera, G. Shi, H. Djieutedjeu, A. Page, C. Uher, E. Kioupakis and P. F. P. Poudeu, *Inorg. Chem.*, 2015, **54**, 746–755.
- 5 J. Casamento, J. S. Lopez, N. A. Moroz, A. Olvera, H. Djieutedjeu, A. Page, C. Uher and P. F. P. Poudeu, *Inorg. Chem.*, 2017, **56**, 261–268.
- 6 M. Ohta, D. Y. Chung, M. Kunii and M. G. Kanatzidis, *J. Mater. Chem. A*, 2014, **2**, 20048–20058.
- 7 S. Sassi, C. Candolfi, V. Ohorodniichuk, C. Gendarme, P. Masschelein, A. Dauscher and B. Lenoir, *J. Electron. Mater.*, 2017, **46**, 2790–2796.
- 8 S. Sassi, C. Candolfi, G. Delaizir, S. Migot, J. Ghanbaja, C. Gendarme, A. Dauscher, B. Malaman and B. Lenoir, *Inorg. Chem.*, 2017, **57**, 422–434.
- 9 K. Segawa, A. A. Taskin and Y. Ando, *J. Solid State Chem.*, 2015, **221**, 196–201.
- 10 K. Nakayama, K. Eto, Y. Tanaka, T. Sato, S. Souma, T. Takahashi, K. Segawa and Y. Ando, *Phys. Rev. Lett.*, 2012, **109**, 236804.
- 11 S. Sasaki, K. Segawa and Y. Ando, *Phys. Rev. B*, 2014, **90**, 220504(R).
- 12 L. Fang, C. C. Stoumpos, Y. Jia, A. Glatz, D. Y. Chung, H. Claus, U. Welp, W.-K. Kwok and M. G. Kanatzidis, *Phys. Rev. B*, 2014, **90**, 020504(R).
- 13 X. Ren, A. K. Singh, L. Fang, M. G. Kanatzidis, F. Tavazza, A. V. Davydov and L. J. Lauhon, *Nano Lett.*, 2016, **16**, 6064–6069.
- 14 L. Shelimova, O. Karpinskii, P. Konstantinov, E. Avilov, M. Kretova, G. Lubman, I. Y. Nikhezina and V. Zemskov, *Inorg. Mater.*, 2010, **46**, 120–126.

- 15 L. Shelimova, O. Karpinskii and V. Zemskov, *Inorg. Mater.*, 2008, **44**, 927–931.
- 16 V. Zemskov, L. Shelimova, P. Konstantinov, E. Avilov, M. Kretova and I. Y. Nikhezina, *Inorg Mater: Applied Res.*, 2011, **2**, 405–413.
- 17 *Thermoelectrics and its Energy Harvesting*, ed. D. M. Rowe, CRC Press, 2012.
- 18 H. J. Goldsmid, in *Thermoelectric Refrigeration*, Temple Press Books, Ltd., London, 1964.
- 19 Y. Zhang, A. P. Wilkinson, P. L. Lee, S. D. Shastri, D. Shu, D.-Y. Chung and M. G. Kanatzidis, *J. Appl. Cryst.*, 2005, **38**, 433–441.
- 20 P.-F. Lory, S. Pailhès, V. M. Giordano, H. Euchner, H. D. Nguyen, R. Ramlau, H. Borrmann, M. Schmidt, M. Baitinger, M. Ikeda, P. Tomes, M. Mihalkovic, C. Allio, M. R. Johnson, H. Schober, Y. Sidis, F. Bourdarot, L. P. Regnault, J. Ollivier, S. Paschen, Yu. Grin and M. de Boissieu, *Nature Comm.* 2017, **8**, 491.
- 21 W. Li and N. Mingo, *Phys. Rev. B*, 2015, **91**, 144304.
- 22 N. English, J. Tse and D. Carey, *Phys. Rev. B*, 2009, **80**, 134306.
- 23 J. Carrete, W. Li, N. Mingo, S. Wang and S. Curtarolo, *Phys. Rev. X*, 2014, **4**, 11019.
- 24 T. Tadano, Y. Gohda and S. Tsuneyuki, *Phys. Rev. Lett.*, 2015, **114**, 95501.
- 25 M. M. Koza, A. Leithe-Jasper, E. Sischka, W. Schnelle, H. Borrmann, H. Mutka and Y. Grin, *Phys. Chem. Chem. Phys.*, 2014, **16**, 27119.
- 26 V. F. Sears, *Neutron News*, 1992, **3**, 26.
- 27 G. Squires, *Introduction to the Theory of Thermal Neutron Scattering*, Dover Publications, Inc., Mineola, New York, 1996.
- 28 S. Lovesey, *Theory of Neutron Scattering from Condensed Matter*, Oxford Science Publications, Oxford, UK, 1984.
- 29 M. M. Bredov, B. A. Kotov, N. M. Okuneva, V. S. Oskotskii and A. L. Shakh-Budagov, *Phys. Solid State*, 1967, **9**, 214.
- 30 V. S. Oskotskii, *Phys. Solid State*, 1967, **9**, 420.

- 31 M. M. Koza, L. Capogna, A. Leithe-Jasper, H. Rosner, W. Schnelle, H. Mutka, M. R. Johnson, C. Ritter and Yu. Grin, *Phys. Rev. B*, 2010, **81**, 174302.
- 32 M. M. Koza, A. Leithe-Jasper, H. Rosner, W. Schnelle, H. Mutka, M. R. Johnson, M. Krisch, L. Capogna and Yu. Grin, *Phys. Rev. B*, 2011, **84**, 014306.
- 33 M. M. Koza, D. Adroja, N. Takeda, Z. Henkie and T. Cichorek, *J. Phys. Soc. Jpn.*, 2013, **82**, 114607.
- 34 V. Keppens, D. Mandrus, B. C. Sales, B. C. Chakoumakos, P. Dai, R. Coldea, M. B. Maple, D. A. Gajewski, E. J. Freeman and S. Bennington, *Nature*, 1998, **395**, 876.
- 35 R. P. Hermann, W. Schweika, O. Leupold, R. Ruffer, G. S. Nolas, F. Grandjean and G. J. Long, *Phys. Rev. B*, 2005, **72**, 174301.
- 36 Y. Takasu, T. Hasegawa, N. Ogita, M. Udagawa, M. A. Avila, K. Suekuni, I. Ishii, T. Suzuki and T. Takabatake, *Phys. Rev. B*, 2006, **74**, 174303.
- 37 M. Christensen, S. Johnsen and B. B. Iversen, *Dalton Trans.*, 2010, **39**, 978.
- 38 J. D. Dunitz, V. Schomaker, and K. N. Trueblood, *J. Phys. Chem.*, 1988, **92**, 856.
- 39 Y. Bouyrie, C. Candolfi, S. Pailhes, M. M. Koza, B. Malaman, A. Dauscher, T. Janusz, O. Boisron, L. Saviot and B. Lenoir, *Phys. Chem. Chem. Phys.*, 2015, **17**, 19751.
- 40 A. F. May, O. Delaire, J. L. Niedziela, E. Lara-Curzio, M. A. Susner, D. L. Abernathy, M. Kirkham and M. A. McGuire, *Phys. Rev. B*, 2016, **93**, 064104.
- 41 H. Mutka, M. M. Koza, M. R. Johnson, Z. Hiroi, J.-I. Yamaura and Y. Nagao, *Phys. Rev. B*, 2008, **78**, 104307.
- 42 D. J. Safarik, T. Klimczuk, A. Llobet, D. D. Byler, J. C. Lashley, J. R. O'Brien and N. R. Dilley, *Phys. Rev. B*, 2012, **85**, 014103.
- 43 D. J. Safarik, A. Llobet and J. C. Lashley, *Phys. Rev. B*, 2012, **85**, 174105.
- 44 M. M. Koza, A. Leithe-Jasper, E. Sischka, W. Schnelle, H. Borrmann, H. Mutka and Y. Grin, *Phys. Chem. Chem. Phys.*, 2014, **16**, 27119.

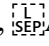
- 45 M. M. Koza, H. Mutka, Y. Okamoto, J.-I. Yamaura and Z. Hiroi, *Phys. Chem. Chem. Phys.*, 2015, **17**, 24837.
- 46 K. Suekuni, M. A. Avila, K. Umeo, and T. Takabatake, *Phys. Rev. B*, 2007, **75**, 195210.
- 47 S. Paschen, W. Carrillo-Cabrera, A. Bentien, V. H. Tran, M. Baenitz, Yu. Grin, and F. Steglich, *Phys. Rev. B*, 2001, **64**, 214404.
- 48 U. Aydemir, C. Candolfi, H. Borrmann, M. Baitinger, A. Ormeci, W. Carrillo-Cabrera, C. Chubilleau, B. Lenoir, A. Dauscher, N. Oeschler, F. Steglich and Yu. Grin, *Dalton Trans.*, 2010, **39**, 1078.
- 49 U. Aydemir, C. Candolfi, A. Ormeci, Y. Oztan, M. Baitinger, N. Oeschler, F. Steglich and Y. Grin, *Phys. Rev. B*, 2011, **84**, 195137.
- 50 A. Bentien, E. Nishikori, S. Paschen and B. B. Iversen, *Phys. Rev. B*, 2005, **71**, 144107.
- 51 U. Aydemir, C. Candolfi, A. Ormeci, M. Baitinger, U. Burkhardt, N. Oeschler, F. Steglich and Yu. Grin, *Dalton Trans.*, 2015, **44**, 7524.
- 52 M. A. Avila, K. Suekuni, K. Umeo, H. Fukuoka, S. Yamanaka and T. Takabatake, *Phys. Rev. B*, 2006, **74**, 125109.
- 53 C. Candolfi, U. Aydemir, M. M. Koza, M. Baitinger, Yu. Grin and F. Steglich, *J. Phys.: Condens. Matter*, 2015, **27**, 485401.

Table Captions

Table 1. Room-temperature equivalent thermal displacement parameters U_{eq} for the five inequivalent positions of the Pb atoms in the $m = 1, 2$ and 3 compounds determined by single crystal X-ray diffraction data (Ref. 8). All the values are expressed in \AA^2 .

Atoms	$U_{eq} (m = 1)$	$U_{eq} (m = 2)$	$U_{eq} (m = 3)$
Pb1	0.0217(4)	0.0198(3)	0.0194(3)
Pb2	0.0220(4)	0.0211(3)	0.0217(3)
Pb3	0.0299(4)	0.0268(3)	0.0259(3)
Pb4	0.0289(4)	0.0280(3)	0.0281(3)
Pb5	0.0300(4)	0.0337(4)	0.0367(4)

Table 2. Values of the fitting parameters inferred from fits to the $C_p(T)$ data shown in Figure 9. In the different models considered, the parameters that were allowed to vary during the least-squares refinements are indicated in parenthesis. For all models, the number of Debye oscillators was kept constant and equal to the sum of the Bi and Se atoms ($N_D = 20, 35$ and 50 for the $m = 1, 2$ and 3 compounds, respectively); only the Pb atoms were considered as Einstein oscillators.

$m = 1$	θ_D (K)	N_{E1}	θ_{E1} (K)	N_{E2}	θ_{E2} (K)
I (θ_D, θ_{E1})	126	3	37.8	/	/
II ($\theta_D, N_{E1}, \theta_{E1}$)	127	3.6	38.8	/	/
III ($\theta_D, \theta_{E1}, \theta_{E2}$)	129	3	36.8	2	59.4
IV ($\theta_D, N_{E1}, \theta_{E1}, N_{E2}, \theta_{E2}$)	127	2.5	38.5	1.1	40
$m = 2$	θ_D (K)	N_{E1}	θ_{E1} (K)	N_{E2}	θ_{E2} (K)
I (θ_D, θ_{E1})	132	3	37.8	/	/
II ($\theta_D, N_{E1}, \theta_{E1}$)	137	5.9	41.4	/	/
III ($\theta_D, \theta_{E1}, \theta_{E2}$)	136	3	40	2	40
IV ($\theta_D, N_{E1}, \theta_{E1}, N_{E2}, \theta_{E2}$)	136	6	42	~0	40
$m = 3$	θ_D (K)	N_{E1}	θ_{E1} (K)	N_{E2}	θ_{E2} (K)
I (θ_D, θ_{E1})	145	9	43.3	/	/
II ($\theta_D, N_{E1}, \theta_{E1}$)	143	8.0	42.5	/	/
III ($\theta_D, \theta_{E1}, \theta_{E2}$)	144	3	37.6	6	47.7
III ($\theta_D, N_{E1}, \theta_{E1}, N_{E2}, \theta_{E2}$)	143	4.7	42	3.2	42

Figure Captions

Fig. 1 (Upper panel) View of the monoclinic unit cell of the $m = 1, 2$ and 3 compounds projected along the b axis. The crystal structure is built from alternate Pb-Se and Bi-Se layers. The Pb, Bi and Se atoms are shown in blue, purple and black, respectively. (Lower panel) Chemical environment of the Pb atoms in the illustrative $m = 1$ compound in ellipsoid representation (98% probability level). Pb exhibits similar environments in the $m = 2$ and 3 compounds.

Fig. 2 Inelastic neutron scattering intensity $S(Q, \omega)$ measured at IN6@ILL at 300 K for the (a) $m = 1$, (b) $m = 2$ and (c) $m = 3$ compounds. The negative energy region corresponds to the anti-Stokes line. The intensity is represented on a linear scale with the maximum intensity limited to unity at the elastic line (visible near 0 eV and up to 0.5 meV). The horizontal white arrows show the position of the main intensity areas while the vertical white arrow marks the position of the dispersion of acoustic phonons that emanates from an intense Bragg peak.

Fig. 3 (a) Generalized vibrational density of states $G(\omega)$ of the $m = 1, 2$ and 3 compounds at 300 K derived from INS measurements on the IN6@ILL spectrometer. The spectra were normalized to 75, 120 and 165 phonon modes for the $m = 1, 2$ and 3 compounds, respectively. (b) Debye plots $G(\omega)/\omega^2$ for the $m = 1, 2$ and 3 compounds that stress the low-energy region of the $G(\omega)$ spectra. The color-coded symbols are similar in both panels.

Fig. 4 Difference spectrum $\Delta G(\omega)$ derived at 300 K from the IN6 data by subtraction of the $m = 1$ from the $m = 3$ inelastic response after normalization of both spectra to the low-energy feature.

Fig. 5 Contrast plots of the dynamic structure factor $S(Q, \omega)$ of the (a and b) $m = 1$ and (c and d) $m = 3$ compounds measured at IN4@ILL at 100 (panels a and c) and 300 K (panels b and d). This positive energy region corresponds to the Stokes line. The intensity is plotted on a linear scale with the maximum intensity limited to unity at the elastic line in order to better visualize the inelastic signal. The horizontal white arrows indicate the position of the peaks identified in $G(\omega)$ inferred from IN6@ILL data. The vertical white arrows indicate the dispersion of acoustic phonons that emanate from strong Bragg peaks.

Fig. 6 Temperature dependence of the generalized vibrational density of states $G(\omega)$ of the (a-d) $m = 1$, (b) 2 and (c-e) 3 compounds measured at IN6@ILL (left panels) and at IN4@ILL (right panels). The temperature- and color-coded symbols are reported in the figures.

Fig. 7 Temperature dependence of the low-energy region of the GVDOS spectra of the (a-d) $m = 1$, (b) 2 and (c-e) 3 compounds measured at IN6@ILL (left panels) and IN4@ILL (right panels). The data below 2 meV have been discarded due to the elastic line contribution that gives rise to an increase in the measured intensity.

Fig. 8 Temperature dependence of the characteristic energy (circle symbols) of the low-energy peak near 4.8 meV obtained from the fit to the $G(\omega)/\omega^2$ data with Gaussian functions. The filled and empty symbols correspond to the IN6 and IN4 data, respectively. The IN6 data have been slightly scaled up to match the IN4 data at 300 K in order to account for the different energy resolution and phase space covered by the two spectrometers. The solid lines are guides to the eye.

Fig. 9 Fit to the specific heat data $C_p(T)$ plotted as $C_p(T)/T^3$ versus T on a logarithmic scale for the $m = 1$ (red filled circles), $m = 2$ (blue filled squares) and $m = 3$ (green filled triangles) compounds using a combination of Debye and Einstein modes as described in the text.

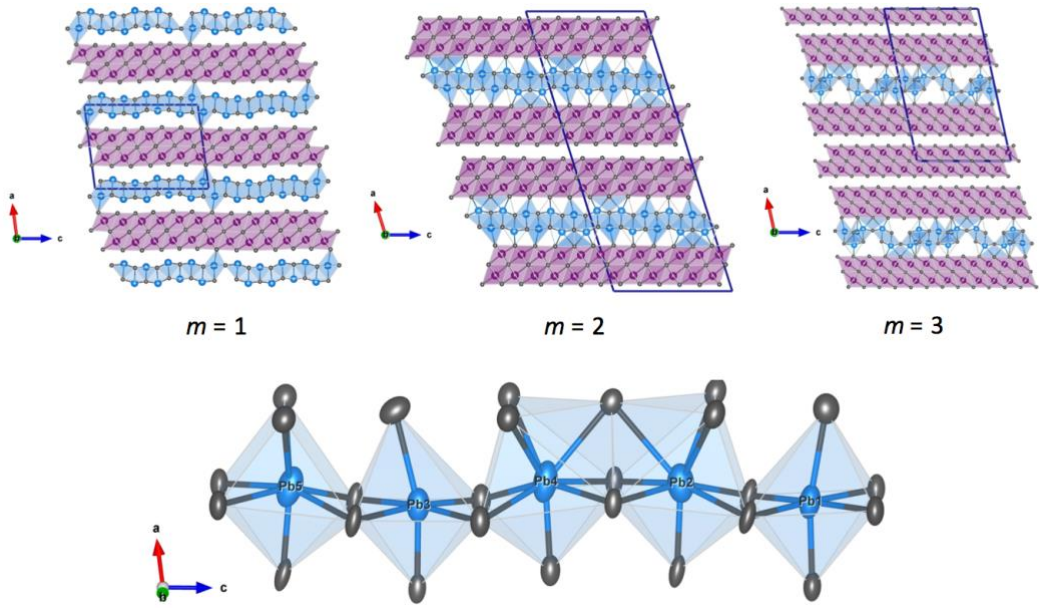


Figure 1

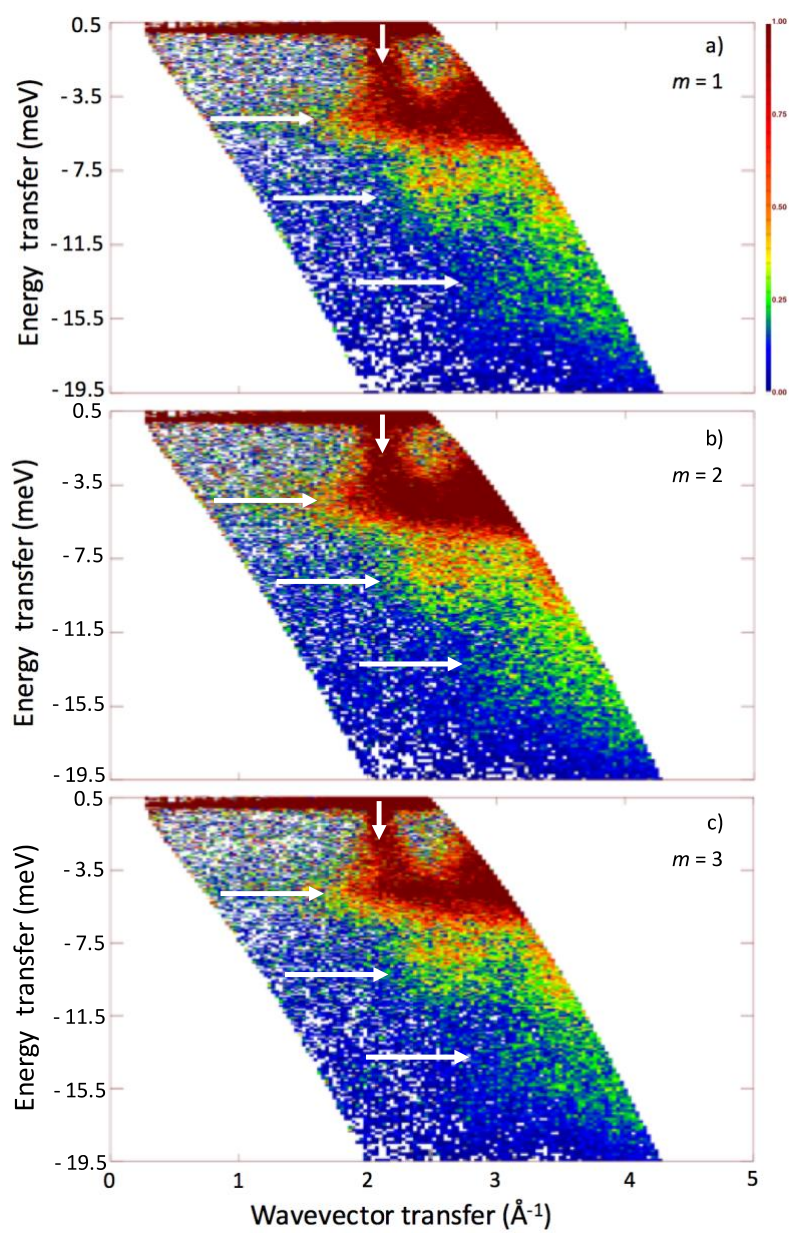


Figure 2

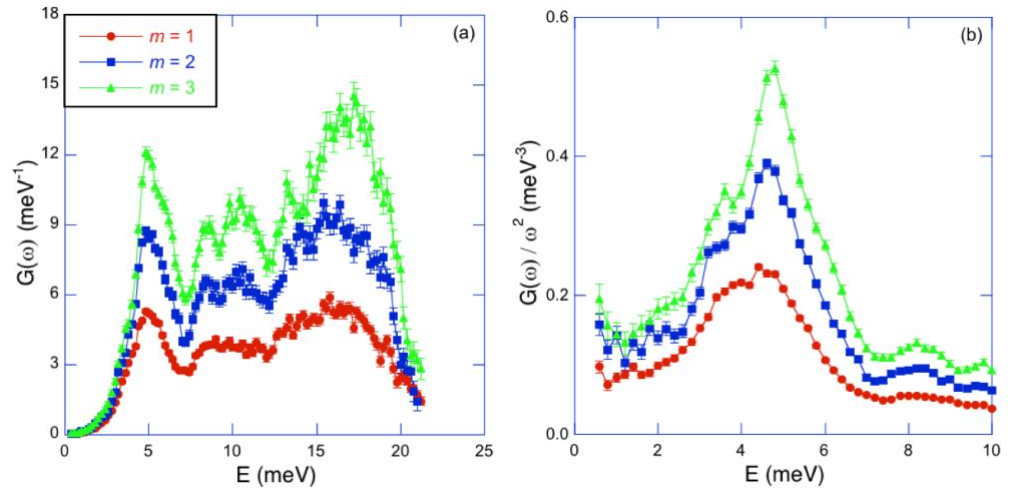


Figure 3

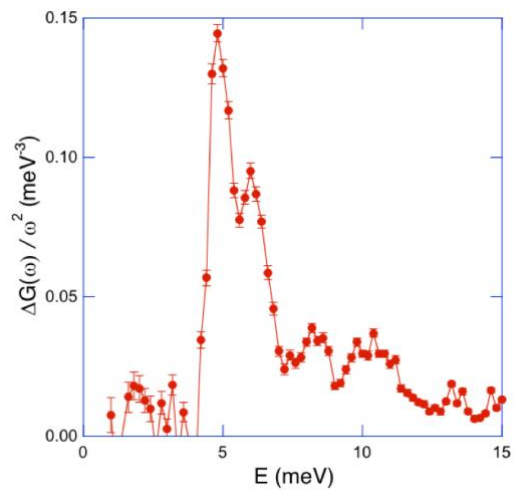


Figure 4

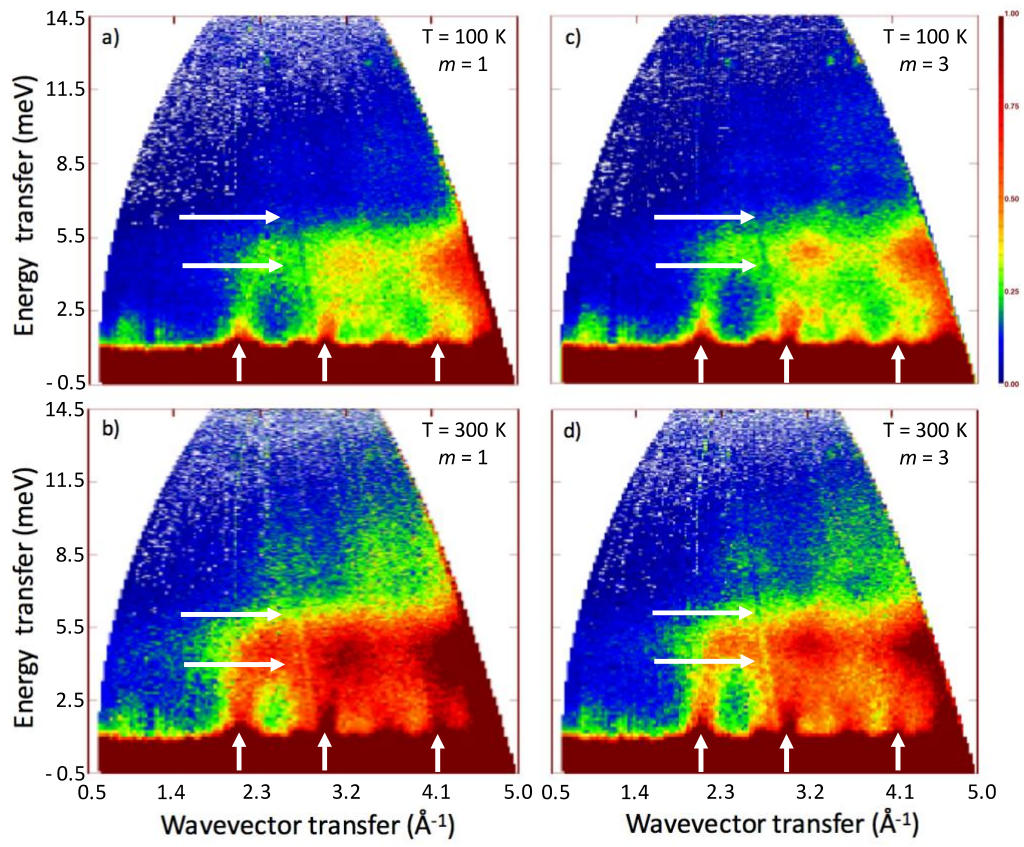


Figure 5

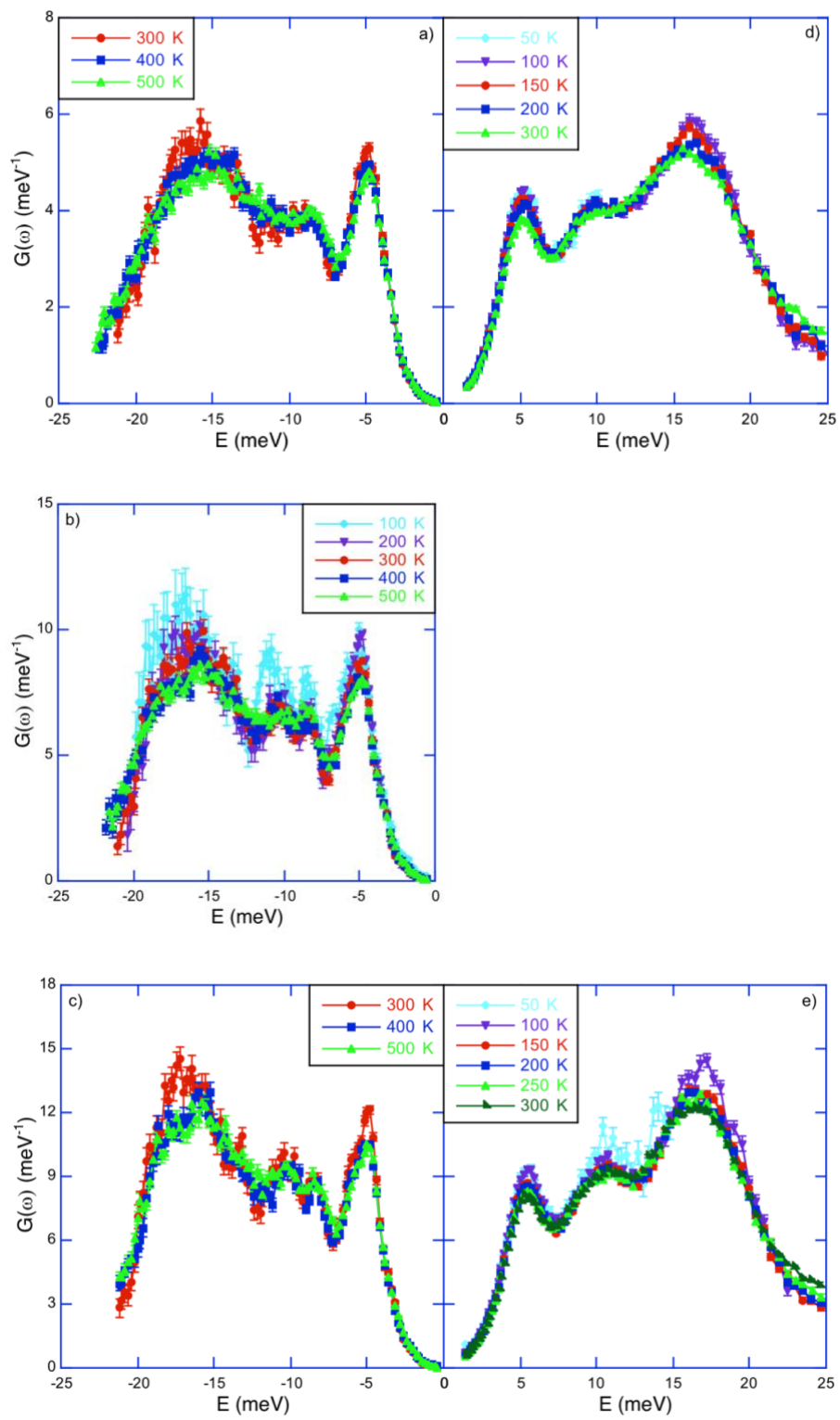


Figure 6

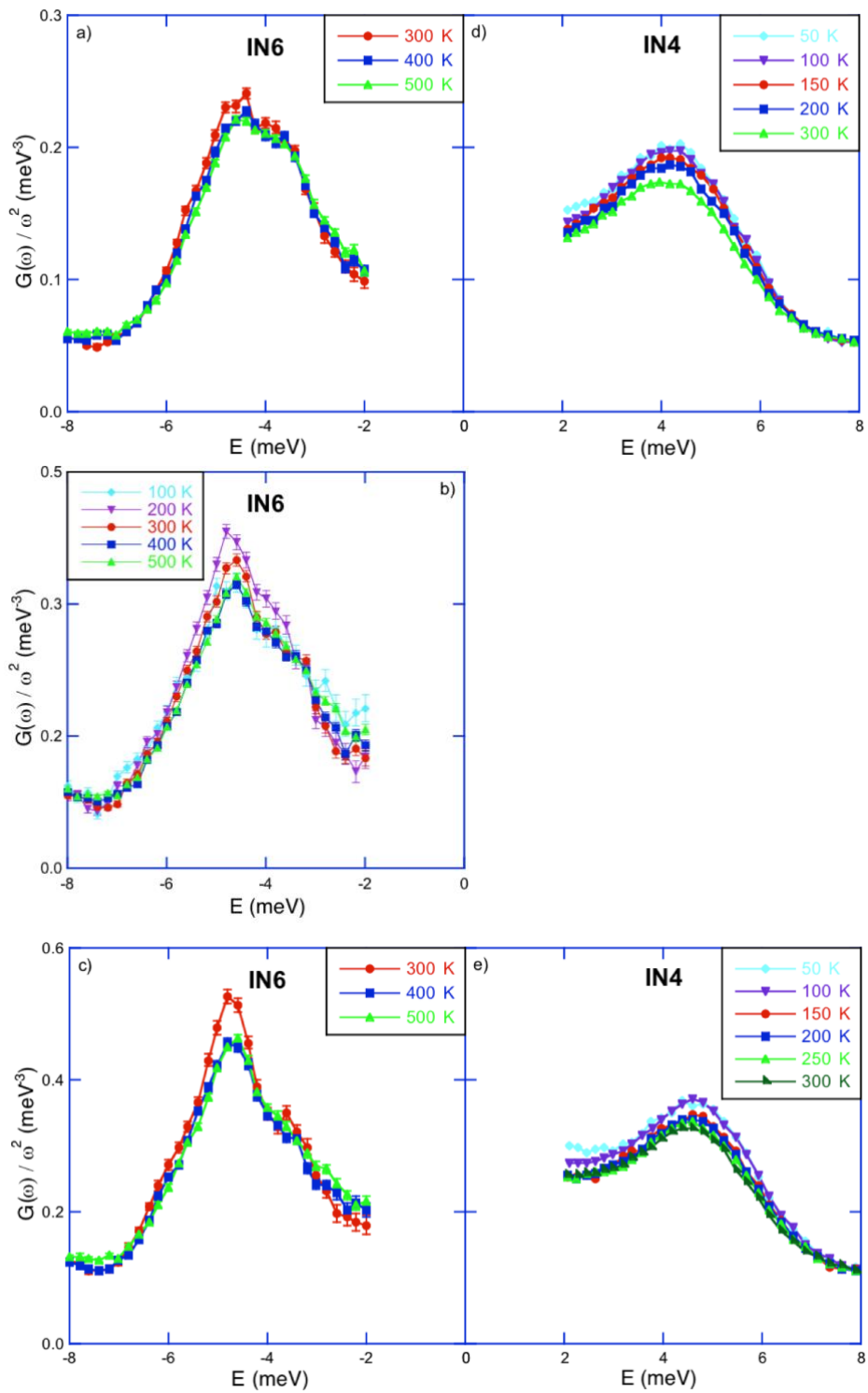


Figure 7

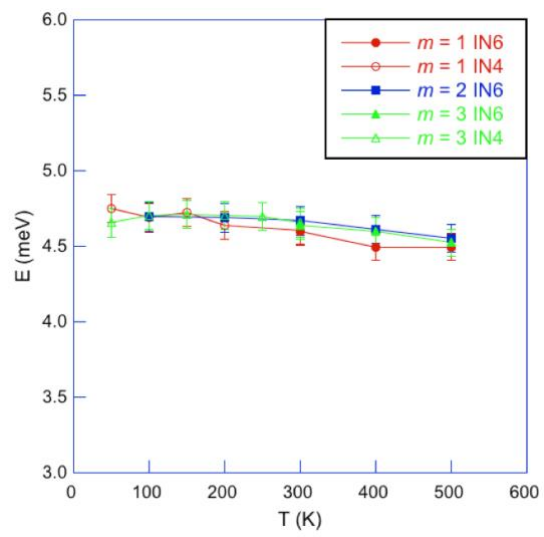


Figure 8

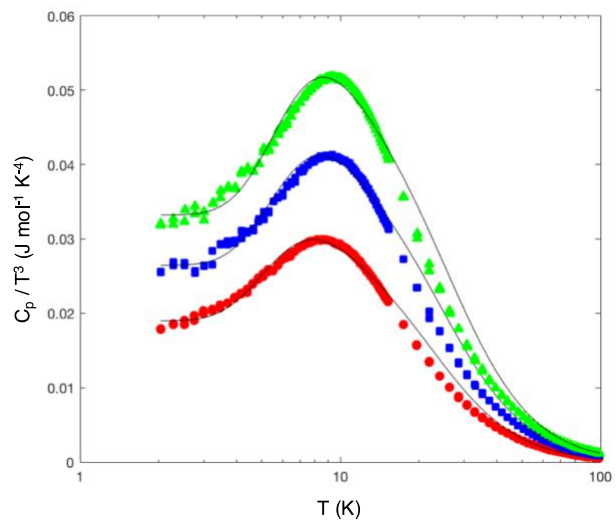


Figure 9